IEEE Access
Multidisciplinary | Rapid Review | Open Access Journal

Received December 11, 2019, accepted December 30, 2019, date of publication January 3, 2020,
date of current version January 14, 2020.

Digital Object Identifier 10.1109/ACCESS.2020.2963953

An Adaptive Matrix Pencil Algorithm Based-Wavelet Soft-Threshold Denoising for Analysis of Low Frequency Oscillation in Power Systems

JIAN CHEN[1,2], XIN LI[3], MOHAMED A. MOHAMED[1,4], (Member, IEEE), AND TAO JIN[1], (Senior Member, IEEE)

[1]Department of Electrical Engineering, Fuzhou University, Fuzhou 350116, China
[2]School of Electrical Information Engineering, Hunan Institute of Technology, Hengyang 421002, China
[3]School of Computer and Information Science, Hunan Institute of Technology, Hengyang 421002, China
[4]Electrical Engineering Department, Faculty of Engineering, Minia University, Minia 61519, Egypt

Corresponding authors: Xin Li (xinl_li@163.com) and Tao Jin (jintly@fzu.edu.cn)

This work was supported in part by the Natural Science Foundation of Hunan Province of China under Grant 2019JJ40063, in part by the Chinese National Natural Science Foundation under Grant 51977039 and Grant 51807031, and in part by the Research Fund for International Young Scientists of the National Natural Science Foundation of China under Grant 51950410593.

ABSTRACT One of the main reasons that affecting the stability of power systems is low frequency oscillation (LFO). The existence of noise influences the accuracy of LFO mode identification extracted from wide-area measurement system (WAMS). The wavelet threshold de-noising is widely used in signal processing. In this paper, wavelet soft threshold is illustrated to attenuate the noise of LFO signal, the optimal wavelet basis and decomposition level for de-noising LFO signal with noise are obtained and verified by experiments. Following the signal de-noising, an improved Matrix Pencil (MP) algorithm is used for mode identification of LFO. This improvement particularly lies in the ratio of adjacent singular entropy increment difference (RASEID) designed as an adaptive order determination method in the MP algorithm proposed in the paper. RASEID not only makes the MP algorithm adaptive, but also enhances the stability of the order determination in the mode identification process. The proposed method ensures the accuracy of mode identification with lower sensitivity to noise interference. Finally, the validity of the proposed method is verified by three cases studies. The first study is on the analysis of synthetic signal typically performed in many literatures. The second study is to identify the mode of active power LFO signal which is generated by IEEE four-generator and two-area system given with disturbance on RT-LAB experimental platform. The third study is the oscillation analysis of the actual LFO data in the North American power grid. The results validate the feasibility of the proposed method for mode identification of noisy LFO.

INDEX TERMS Low-frequency oscillation (LFO), wavelet soft-threshold de-noising, ratio of adjacent singular entropy increment difference (RASEID), adaptive, Matrix Pencil (MP), RT-LAB platform.

I. INTRODUCTION

It is well known that low-frequency oscillation (LFO) is an inherent phenomenon of power systems [1]. The large-capacity and long-distance power transmission weaken the damping characteristics of the system, while small-scale disturbances of generating units and lines result in LFO of the power grid [2]. Since LFO restricts the capacity of power transmission and even causes a blackout in serious situations of power systems, it is important to identify the LFO modes so as to take appropriate strategy for suppressing LFO [3], [4].

There are two main research methods for LFO modal analysis of power systems: one is based on model [1], [5] that is, the differential and algebraic equations of the whole system are set up by establishing the electromechanical transient model of each component, and the stability of the system

The associate editor coordinating the review of this manuscript and approving it for publication was Min Wang.

is analyzed according to Lyapunov's first stability theorem. However, this method is only suitable for off-line analysis which depends on the accuracy of the model and parameters. Therefore, it is not suitable for the analysis of large-scale and high-order systems [6], [7]. The other method is based on real-time measuring information which has developed with the promotion and application of wide-area measurement systems (WAMS) in the past decade [8]–[10]. The latter uses advanced mathematical algorithms to analyze the LFO of power systems.

The autoregressive moving average (ARMA) algorithm [11] determines the order of the model by a large number of trial calculations on different order models, which limits the online application value of this kind of methods. In [12], fast Fourier transform (FFT) algorithm is introduced to analyze the power system data with noise. The algorithm has high accuracy and good robustness, but it is unable to fully identify the oscillation mode parameters. In [13], the wavelet ridge algorithm is used to deal with time-varying oscillation signals, which is of great significance in the field of LFO. However, the resolution of this algorithm is not high when extracting multi-frequency component signals. Hilbert-Huang transform (HHT) method is introduced in [14], which is particularly effective for non-linear and non-stationary signal analysis. However, in the process of analysis, there will be endpoint effect and modal aliasing, which has undesired impact on the identification effect. The Prony algorithm uses the linear combination of exponential functions to describe the mathematical model of sampling data with equal spacing. However, Prony algorithm can't get accurate oscillation mode parameters since it is greatly affected by noise [15]. The total least squares-estimation of signal parameters via rotational invariance techniques (TLS-ESPRIT) method needs to operate the singular value decomposition (SVD) twice in the calculation which increases computational complexity [16]. Matrix Pencil (MP) is a representative and powerful one in these modern mode identification algorithms [17], [18]. Nonetheless, How to determine the order of SVD is the critical problem of the MP algorithm. The conventional threshold setting of order determination is influenced by human experience and is not self-adaptive. Although literatures [7], [19] enhance the adaptability of this algorithm to determine the order, their performance of noise resistance and accuracy need further verification. Hence, it is necessary to develop and enrich the novel methods for order determination.

Prior mode identification, the LFO physical parameters such as voltage, power, etc. are collected with phasor measurement units (PMU) installed at each node of the power grid. However, measurement noise and communication error may cause erroneous data in the transmitting from PMU to the central station of WAMS. In the context of extracting the LFO signal, the data probably submerge, especially in the situation of strong noise and the mode identification of the LFO signal will be difficult or unfeasible. Therefore, it is critical to take a measurement for the noise reduction of LFO.

The key of noise reduction preprocessing is to filter the noise without distortion as much as possible and purify the real LFO signal from WAMS [19]. In the traditional de-noising method, FFT uses the signal transform between time domain and frequency domain to filter the noise, which is suitable for the situation that the effective signal and noise belong to different frequency bands. However, this method is difficult to work since the actual white noise exists in the whole frequency band. The digital filter, such as low-pass filter, has the problems of time-delay and distortion caused by nonlinear phase-shift. It can't effectively filter out the noise, when the noise and the monitoring signal spectrum are overlapped.

With the development and perfection of modern signal processing, the means of noise reduction are greatly enriched. Kalman filter (KF) requires a good dynamic model and the model is generally complex, which brings difficulties to its popularization and application [20], [21]. The empirical mode decomposition (EMD) method produces mode aliasing and requires high calculation time [22], [23]. In [24], [25], the method of fuzzy filtering is used for filtering. The advantage of this method is that the parameters of the filter do not need to be determined and the operation process is simple. However, it lacks self-adaptability and is not suitable for all noisy signals. In [26], the filter based on the adaptive neuro-fuzzy inference system (ANFIS) is complex and it is difficult to establish the membership function of the algorithm. In [27], [28] the performance of morphological filter depends on the type of morphological transformation, the shape and size of structural elements. That is to say, if the size of the structural elements is too small, the effect of noise reduction is unsatisfactory. Conversely, if the size of the structural elements is too large, the structure of the signal will be damaged and the characteristics of the signal will be damaged which makes it difficult to choose the best parameter. The authors in [29] shows that wavelet de-noising has a wide range of function adaptability and the best adaptive de-noising ability. As a modern signal processing method, the wavelet soft-threshold de-noising method is widely used in practical applications [7], [30]–[37]. However, there are many kinds of wavelet bases such as DbN, Coif$N$, Sym$N$, etc. There are different filtering effects with different wavelet bases and decomposition levels to some special signals. Therefore, it is important to research on the optimization of wavelet basis and decomposition level for LFO signal.

The main contributions in this paper are summarized as follows:

- Most of the wavelet bases in MATLAB toolboxes are tested to filter the noisy LFO signal and the best matching one is chosen to perform for the noise reduction of LFO signal. On the other hand, a proper number of decomposition levels is studied and determined according to the de-noising effect.
- Ratio of adjacent singular entropy increment difference (RASEID) is proposed to solve the adaptive problem

in MP algorithm, which improves the accurate order determination ability of the MP algorithm for noisy LFO signals. Moreover, it can improve the accuracy and adaptability of LFO mode identification of the MP algorithm.

- The LFO in the IEEE four-generator and two-area system is experimentally analyzed and the proposed method in the paper is validated by RT-LAB experiment platform. To the best of our knowledge, this platform has not been pointed out in any similar work.

The rest of the paper is organized as follows: Section 2 briefly summarizes the principle of wavelet soft-threshold de-noising. Furthermore, the performance of different wavelet bases and decomposition levels are tested and compared to choose the best parameters matching the noise reduction of LFO signal. In Section 3, the order determination method, RASEID is described and used to make the order determination adaptive in MP algorithm for identifying the LFO signal. In Section 4, three cases studies are performed to validate the proposed method. The first case study is about mode identification of a synthetic test signal. The second one concern the LFO data generated in the RT-LAB experiment platform and compares the effect of different identifying methods. The third one is the oscillation analysis of the actual LFO data in the North American power grid. Finally, Section 5 addresses the conclusion of the paper.

II. WAVELET SOFT-THRESHOLD DE-NOISING

The basic principle of wavelet soft-threshold de-noising is briefly introduced in subsection A. In subsection B and C, the selections of wavelet basis and decomposition level are experimentally studied and summarized which are two critical problems in the de-noising process. Then, the optimal matching of wavelet basis and decomposition level is obtained for LFO de-noising which is conducive to the accuracy of LFO mode identification.

A. THE PRINCIPLE OF WAVELET SOFT-THRESHOLD DE-NOISING

The actual LFO signal extracted from WMAS is described as follows:

$$\boldsymbol{x}(n) = \boldsymbol{s}(n) + \boldsymbol{g}(n) \tag{1}$$

where $\boldsymbol{x}(n)$ stands for noisy LFO signal, $\boldsymbol{s}(n)$ denotes original LFO signal unpolluted, $\boldsymbol{g}(n)$ is the white Gaussian noise signal. $n = 0, 1, 2, \cdots, N\text{-}1$ and N is the length of $\boldsymbol{x}(n)$. The method of wavelet soft-threshold de-noising proposed by Donoho et al. [29] is simply described as follows:

$$\boldsymbol{W}_x(j,k) = \boldsymbol{W}_s(j,k) + \boldsymbol{W}_g(j,k) \tag{2}$$

where $\boldsymbol{W}_x(j,k)$, $\boldsymbol{W}_s(j,k)$ and $\boldsymbol{W}_g(j,k)$ represent the wavelet transform of $\boldsymbol{x}(n)$, $\boldsymbol{s}(n)$ and $\boldsymbol{g}(n)$ respectively. j is the number of decomposition levels, and k is the order of the wavelet coefficient. The wavelet decomposition coefficients of $\boldsymbol{s}(n)$ are mainly concentrated in some primary coefficients. The energy distribution of $\boldsymbol{g}(n)$ is dispersed in the whole domain of wavelet decomposition and the corresponding decomposition coefficients are small. To attenuate noise, a suitable threshold T is set by:

$$T = \rho\sqrt{2\ln N} \tag{3}$$

where ρ is the standard deviation of $\boldsymbol{x}(n)$. The actual situation is that the noise is unknown, so the parameter ρ should be estimated by the following equation:

$$\rho = \text{Median}(|w_{j,k}|)/0.6745 \tag{4}$$

where $w_{j,k}$ denotes the j-th level and k-th wavelet coefficient in the wavelet transform. $|\cdot|$ is to get the absolute value of $w_{j,k}$. Median $(\cdot)$ denotes a function that takes the median of the sequence in the parenthesis. The value 0.6745 is the adjustment coefficient of standard deviation [29]. The wavelet coefficients are performed to be zeroes which represent the noise, if they are less than T. On the contrary, the wavelet coefficients are shrunk to zero according to a fixed quantity by the function Sgn $(\cdot)$, performed in Equation (5) as follow:

$$\tilde{w}_{j,k} = \begin{cases} \text{Sgn}\left(w_{j,k}\right)\left(\left|w_{j,k} - T\right|\right), & \left|w_{j,k}\right| \geq T \\ 0, & \left|w_{j,k}\right| < T \end{cases} \tag{5}$$

where $\tilde{w}_{j,k}$ denotes the coefficients after wavelet soft-threshold processing.

Including the de-noising steps summarized above, Figure 1 illustrates the process of wavelet soft-threshold de-noising in which the problems 1# and 2# are marked and emphasized in the blue part. The problem 1# is which wavelet basis to select. The selection of a wavelet basis is usually determined with the application, that is, the best wavelet basis selected is according to the different types of signal de-noising. It is better to achieve this goal adaptively, but the selection of wavelet basis is difficult to summarize into general principles, and only specific principles can be put forward for specific problems. On the other hand, problem 2# is the selection of the wavelet decomposition level which is also another important factor worth regarding in the process of the signal de-noising. However, there is no standard method but artificial experience to select the wavelet decomposition level for the best de-noising effect. For pre-setting the decomposition level, the high decomposition level will decrease the

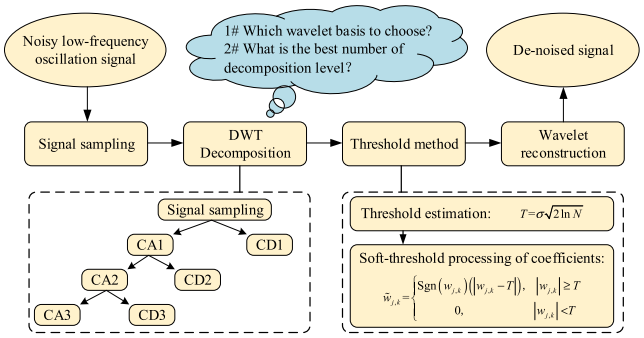

FIGURE 1. The process of wavelet soft-threshold de-noising.

TABLE 1. Comparison of de-noising effects with the best match of different wavelet bases.

Indexes	Haar	Db9	**Coif5**	Sym6	Bior6.8	Rbio6.8
SNR (dB)	17.2045	23.8851	**23.9441**	23.9109	23.8575	23.9002
MSE	0.0203	0.0044	**0.0043**	0.0044	0.0044	0.0044
C_t(s)	1.5524	1.8580	**1.8180**	1.7477	2.0714	2.0997

signal-to-noise ratio (SNR) and lead to the loss of useful signal information, along with increasing the computational workload. On the contrary, if the wavelet decomposition level is too low, the SNR cannot be greatly improved. In order to determine the best parameters more reasonably in the process of wavelet soft-threshold de-noising for LFO signal, the studies on the selections of the best wavelet basis and wavelet decomposition level are carried out in the paper.

B. THE SELECTION OF WAVELET BASIS

The classical LFO signal unpolluted is assumed as follow:

$$\begin{aligned} \boldsymbol{s}(n) = {} & 2.0000 \times e^{-0.2000n} \cdot \cos(2\pi \times 1.5000n) \\ & + 1.5000 \times e^{-0.1000n} \cdot \cos(2\pi \times 0.5000n + \pi/6) \\ & + 0.5000 \times e^{-0.0500n} \cdot \cos(2\pi \times 0.2000n + \pi/3) \end{aligned} \tag{6}$$

where $n = 0, 1, 2, \cdots, N-1$ and N is the length of $\boldsymbol{s}(n)$ which is added with white Gaussian noise $\boldsymbol{g}(n)$ artificially to form $\boldsymbol{x}(n)$ described as Equation (1). As performed in [19], the SNR and mean-square-error (MSE) are presented to evaluate the de-noising effect. The white Gaussian noise is added to $\boldsymbol{s}(n)$ which forms a certain SNR of 15 dB.

The selection of wavelet basis in wavelet de-noising is usually based on the actual de-noising effect of different wavelet bases. In this paper, the best wavelet basis is evaluated and selected according to the evaluating indexes SNR and MSE after de-noising. In fact, most of the wavelet bases including Haar, Daubechies, Biorthogonal, Reversebior, Coiflets, Symlets support discrete wavelet transform (DWT) in MATLAB2017a. In order to analyze and select the best wavelet bases for LFO de-noising, the number of wavelet decomposition levels is assumed to be 3. All these wavelet bases are tested to the same noisy LFO signal $\boldsymbol{x}(n)$ so that the best wavelet basis will be found and selected according to the maximal SNR and the minimal MSE. Table 1 shows the SNR, MSE and C_t of the best type of each wavelet basis. C_t stands for the total operating time to de-noise the signal 1000 realizations. It is illustrated that Coif5 is the best wavelet basis to obtain the maximal SNR and minimal MSE.

C. THE BEST NUMBER OF DECOMPOSITION LEVEL

The wavelet soft-threshold de-noising with wavelet basis Coif5 is utilized to reduce the noise of the LFO signal with SNR of 15 dB. In the context, different decomposition levels based on wavelet basis Coif5 are tested and checked out

TABLE 2. Comparison of de-noising effects with different wavelet decomposition levels.

Decomposition levels	SNR (dB)	MSE	C_t(s)
1	17.9985	0.0169	1.3488
2	20.9615	0.0086	1.6431
3	23.9100	0.0044	1.7839
4	**26.4449**	**0.0024**	**1.9998**
5	22.4326	0.0062	2.2561
6	21.2392	0.0081	2.5478
7	20.7222	0.0091	2.8494
8	20.3382	0.0099	3.0773

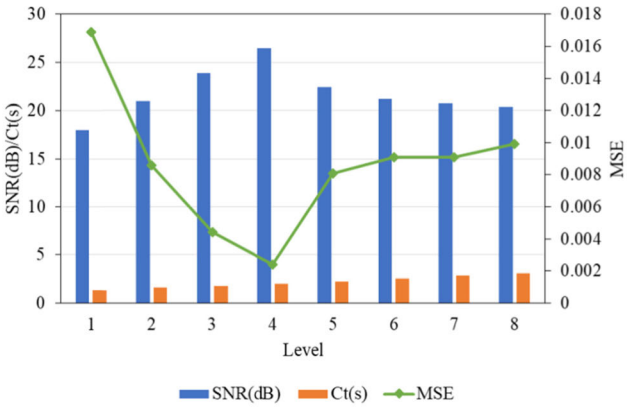

FIGURE 2. SNR, C_t and MSN with different decomposition levels.

which are listed in Table 2. It shows that the best number of composition level with maximal SNR and minimal MSE is level 4. The calculating time C_t of 1000 realizations in different decomposition levels increases with the raise of decomposition level.

The SNR and MSE matching with different decomposition levels listed in Table 2 are also illustrated in Figure 2. The blue square columns indicate the location of the maximal SNR at level 4 as well as the location of minimum MSE depicted in the green line. Therefore, level 4 is the best selection for the decomposition level. On the other hand, taking into account of calculating time, the corresponding calculating time C_t at level 4 is moderate compared with other decomposition levels. Based on the above discussion, wavelet basis Coif5 and decomposition level 4 are the best parameter matching way and have obvious advantages of wavelet soft-threshold de-noising to the noisy LFO signal.

III. ADAPTIVE MP ALGORITHM

In general, the noise intensity which is characterized in SNR is unknown for the LFO signal to be identified. The conventional method of order determination is to set different thresholds artificially according to the experience, so as to determine the order after SVD decomposition. However, the order number is largely influenced by subjective factors inconveniently and it may even cause large errors.

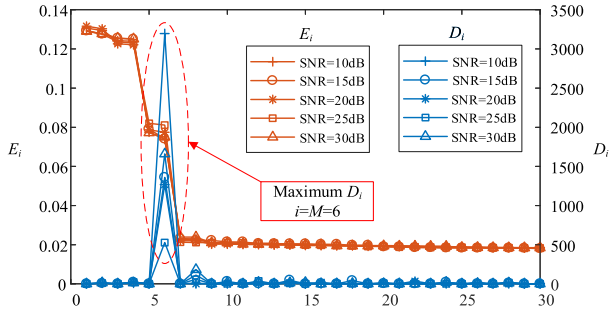

FIGURE 3. Interpretation of RASEID.

Therefore, this paper presents an adaptive order determination method which is designed as RASEID for this problem.

A. THE INTERPRETATION OF RASEID

The singular value sequence of SVD is arranged in non-increasing denoted as follow:

$$\sigma_1 \geq \sigma_2 \geq \cdots \geq \sigma_{i-1} \geq \sigma_i \geq \sigma_{i+1} \geq \cdots \geq \sigma_{L+1} \to 0 \quad (7)$$

where σ_i is the singular value of each order in the SVD and i denotes $1, 2, \cdots, L+1$ respectively. $L+1$ is the total number of singular values. The singular entropy increment denoted by E_i is defined by:

$$E_i = -\frac{\sigma_i}{\sum_{i=1}^{L+1} \sigma_i} \cdot \lg \frac{\sigma_i}{\sum_{i=1}^{L+1} \sigma_i} \quad (8)$$

Then, RASEID designed as the order determination method proposed in this paper is defined as follow:

$$D_i = (E_i - E_{i+1})/(E_{i+1} - E_{i+2}), \quad 1 \leq i \leq L-1 \quad (9)$$

E_i reflects the entropy increment of the corresponding singular value, and D_i reflects the fluctuation of entropy increment at the corresponding order. If D_M is the maximum value of D_i, the actual order will equal to M. This is because its previous orders represent effective signal while the subsequent orders after M represent the noise signal. Since the cumulative percentage increments of the singular values before and after order M are on different orders of magnitude, the maximum value D_M appears on the distribution of D_i. Therefore, D_M depicts the order of the true modes. The distribution of E_i and D_i is schematically illustrated in Figure 3, where $M = 6$ is taken as an example in Figure 3. In addition, the distributions of E_i and D_i with different SNRs are also analyzed and described, which shows the same order $M = 6$ adaptively. Furthermore, Table 3 gives the comparison on the order results gotten by the conventional method EMO / MEMO [38], [39] and the RASEID proposed in the paper. The parameter δ is the sensitivity factor (ranging between 2 and 5) and A_d represents the adaptive threshold. It can be easily noticed that there is no need to set the threshold value in EMO / MEMO and RASEID to determine the order adaptively and accurately. In addition, RASEID has the advance of simplicity to determine the order adaptively and is different with EMO/MEMO which depends on the extra validation condition related to the parameter δ.

TABLE 3. Comparison of order determination in different methods.

Method	Threshold value	Order	Real mode
Conventional method	0.01	291	3
	0.03	34	
EMO / MEMO(δ=5)	A_d	6	
RASEID	A_d	6	

TABLE 4. Accuracy test of RASEID in 1000 realizations.

SNR (dB)	Accurate order determination number	Accuracy rate (%)	Interval of accuracy rate
5	892	89.2	<90%
10	946	94.6	90%~95%
15	973	97.3	95%~98%
20	986	98.6	98%~99%
25	992	99.2	>99%
30	997	99.7	
35	998	99.8	
40	998	99.8	

B. NOISE REJECTION OF RASEID

In subsection A, the order determination principle of RASEID is described. However, in face of different ranks of SNRs, RASEID is not always accurate. Therefore, the rank of SNRs after de-noising effectively ensuring the accuracy of order determination is worth considering. That is, the performance of noise rejection of RASEID should be studied. In this way, the SNR value after de-noising can be used as a judgment before mode identification. To test the accuracy of RASEID, Monte Carlo analysis to the LFO signal presented in Equation (6) is performed. The accuracies of order determination are tested after adding white Gaussian noise with different SNRs of 5 dB to 40 dB in 1000 realizations. Through experiments and statistics, the accuracy performance of the proposed method is tested and given in Table 4. According to the data of Table 4, if the SNR increases to more than 25 dB, the accuracy rate can be large enough over 99%. In addition, it can be seen that the accuracy of adaptive order determination can be improved with the increase of SNR.

C. AN ADAPTIVE MP ALGORITHM

The LFO signal after wavelet soft-threshold de-noising is described by:

$$\hat{\boldsymbol{x}}(n) = \boldsymbol{s}(n) + \boldsymbol{r}(n) = \sum_{i=1}^{P} A_i e^{\alpha_i T_s n} \cos(2\pi f_i T_s n + \theta_i) + \boldsymbol{r}(n) \quad (10)$$

where $n = 0, 1, 2, \cdots, N-1$ and N is the length of the discrete LFO signal. T_s is the sampling period. $\boldsymbol{s}(n)$ is the original LFO signal, $\boldsymbol{r}(n)$ is the residual noise and $\hat{\boldsymbol{x}}(n)$ is assumed to be the actual LFO signal composed of $\boldsymbol{s}(n)$ and

$\boldsymbol{r}$(n). A_i, α_i, f_i and θ_i denote the initial amplitude, damping factor, frequency, and initial phase of each mode respectively. P is the number of LFO signal modes. Equation (10) can be organized as follow:

$$\hat{\boldsymbol{x}}(n) = \boldsymbol{s}(n) + \boldsymbol{r}(n) = \sum_{i=1}^{2P} B_i z_i^n + \boldsymbol{r}(n) \tag{11}$$

where $B_i = \frac{1}{2}A_i e^{j\theta_i}$ and $z_i = e^{(\alpha_i + j2\pi f_i)T_s}$. $2P$ denotes the order number, usually doubling the actual modes number of LFO signal. The steps of adaptive MP algorithm are illustrated as follows:

1) CONSTRUCTING HANKEL MATRIX $\boldsymbol{H}$

The Hankel matrix $\boldsymbol{H}$ is constructed with the order of $(N - L) \times (L + 1)$ using the LFO signal $\hat{\boldsymbol{x}}(n)$ as follow:

$$\boldsymbol{H} = \begin{bmatrix} \hat{x}(0) & \hat{x}(1) & \cdots & \hat{x}(L) \\ \hat{x}(1) & \hat{x}(2) & \cdots & \hat{x}(L+1) \\ \vdots & \vdots & \ddots & \vdots \\ \hat{x}(N-L-1) & \hat{x}(N-L) & \cdots & \hat{x}(N-1) \end{bmatrix} \tag{12}$$

where N is the length of the discrete LFO signal, as illustrated in Equation (10). L equals N/3 in this paper and represents MP parameters, generally designed in the range of $N/4$ to $N/3$.

2) SVD AND ITS ORDER DETERMINATION USING RASEID

The Hankel matrix $\boldsymbol{H}$ is decomposed by SVD as follow:

$$\boldsymbol{H} = \boldsymbol{U}\boldsymbol{\Sigma}\boldsymbol{V}^{\boldsymbol{T}} \tag{13}$$

where $\boldsymbol{U}$ is an orthogonal $(N - L) \times (N - L)$ matrix. $\boldsymbol{V}$ is another orthogonal $(L + 1) \times (L + 1)$ matrix and $\boldsymbol{V}^{\boldsymbol{T}}$ is the conjugate transpose of $\boldsymbol{V}$. $\boldsymbol{\Sigma}$ is a diagonal $(N - L) \times (L + 1)$ matrix, whose principal diagonal elements are illustrated in Equation (7). Using the order determination of RASEID described in subsection A, the actual modal order of $\boldsymbol{\Sigma}$ is assumed to be $2P$. Thus, a new matrix $\boldsymbol{\Sigma}'$ is constructed by the first $2P$ columns of $\boldsymbol{\Sigma}$ as follow:

$$\boldsymbol{\Sigma}' = \begin{bmatrix} \sigma_1 & 0 & \cdots & 0 \\ 0 & \sigma_2 & \cdots & 0 \\ \vdots & \vdots & \ddots & \vdots \\ 0 & 0 & \cdots & \sigma_{2P} \\ & \mathbf{0}_{(N-L-2P)\times 2P} & & \end{bmatrix} \tag{14}$$

where $\boldsymbol{\Sigma}'$ is a $(N-L)\times 2P$ matrix. The first $2P$ rows of $\boldsymbol{\Sigma}'$ for a diagonal matrix containing the diagonal elements of $\sigma_1, \sigma_2, \cdots, \sigma_{2P}$, and the rest elements are filled with zeroes. Obviously, the purpose of constructing a smaller diagonal matrix $\boldsymbol{\Sigma}'$ is to reduce the influence of noise and the complexity of subsequent calculation.

3) CONSTRUCTING THE MATRIX PENCIL $\boldsymbol{Y}_2 - \lambda \boldsymbol{Y}_1$

First, the two matrices of $\boldsymbol{V}_1$ and $\boldsymbol{V}_2$ are to be constructed. According to the order number of $2P$, the first $2P$ columns of $\boldsymbol{V}$ form the matrix $\boldsymbol{V}'$ with the order of $(L + 1) \times 2P$. Then, the last row of $\boldsymbol{V}'$ is deleted to form the matrix $\boldsymbol{V}_1$ with the order of $L \times 2P$ and the first row of $\boldsymbol{V}'$ is deleted to construct $\boldsymbol{V}_2$ with the order of $L \times 2P$. Thus, the following two matrices $\boldsymbol{Y}_1$ and $\boldsymbol{Y}_2$ are constructed as follow [40]:

$$\boldsymbol{Y}_1 = \boldsymbol{U}\boldsymbol{\Sigma}'\boldsymbol{V}_1^{\boldsymbol{T}} \tag{15}$$

$$\boldsymbol{Y}_2 = \boldsymbol{U}\boldsymbol{\Sigma}'\boldsymbol{V}_2^{\boldsymbol{T}} \tag{16}$$

where $\boldsymbol{Y}_1$ and $\boldsymbol{Y}_2$ are two $(N - L) \times L$ matrices.

Furthermore, according to Equation (15) and Equation (16), the matrix pencil $\boldsymbol{Y}_2 - \lambda \boldsymbol{Y}_1$ can be described by [41]:

$$\boldsymbol{Y}_2 - \lambda \boldsymbol{Y}_1 = \boldsymbol{Z}_1 \boldsymbol{B} (\boldsymbol{Z}_0 - \lambda \boldsymbol{I}) \boldsymbol{Z}_2 \tag{17}$$

where λ is a scalar variable. $\boldsymbol{Z}_0$ is a diagonal matrix with the diagonal elements of $\sigma_1, \sigma_2, \cdots, \sigma_{2P}$. $\boldsymbol{B}$ is a diagonal matrix with the diagonal elements of $B_1, B_2, \cdots, B_{2P}$. $\boldsymbol{Z}_1 = \begin{bmatrix} 1 & 1 & \cdots & 1 \\ z_1 & z_2 & \cdots & z_{2P} \\ \vdots & \vdots & \ddots & \vdots \\ z_1^{N-L-1} & z_2^{N-L-1} & \cdots & z_{2P}^{N-L-1} \end{bmatrix}$, $\boldsymbol{Z}_2 = \begin{bmatrix} 1 & z_1 & \cdots & z_1^{L-1} \\ 1 & z_2 & \cdots & z_2^{L-1} \\ \vdots & \vdots & \ddots & \vdots \\ 1 & z_{2P} & \cdots & z_{2P}^{L-1} \end{bmatrix}$ where z_i is the pole of the i-th mode and B_i represents the initial amplitude of the i-th mode and there is a relation of $|B_i| = \frac{1}{2}A_i$, $i = 1, 2, \cdots, 2P$.

4) CALCULATING THE GENERALIZED EIGENVALUES AND OBTAINING α_i AND f_i

In Equation (17), since the signal pole z_i is the generalized eigenvalue of $\boldsymbol{Y}_2 - \lambda \boldsymbol{Y}_1$, the problem of calculating z_i can be transformed into the problem of calculating the eigenvalue of the matrix $\boldsymbol{C}$ as follow:

$$\boldsymbol{C} = \boldsymbol{Y}_1^{+}\boldsymbol{Y}_2 = (\boldsymbol{Y}_1^{T}\boldsymbol{Y}_1)^{-1}\boldsymbol{Y}_1^{T}\boldsymbol{Y}_2 \tag{18}$$

where $\boldsymbol{Y}_1^{+}$ represents the generalized inverse matrix of $\boldsymbol{Y}_1$.

The eigenvalues z_i can be calculated through Equation (18). Since z_i equals $e^{(\alpha_i + j2\pi f_i)T_s}$, that is $\frac{\ln z_i}{T_s} = \alpha_i + j2\pi f_i$ illustrated in Equation (11), α_i and f_i can be calculated by:

$$\begin{cases} \alpha_i = Re[(\ln z_i)/T_s] \\ f_i = \dfrac{1}{2\pi T_s} Im(\ln z_i) \end{cases} \tag{19}$$

5) CALCULATING A_i AND θ_i

Ignoring the influence of noise $\boldsymbol{r}(n)$, Equation (11) can be rewritten as follow:

$$\begin{bmatrix} \hat{x}(0) \\ \hat{x}(1) \\ \vdots \\ \hat{x}(N-1) \end{bmatrix} = \begin{bmatrix} 1 & 1 & \cdots & 1 \\ z_1 & z_2 & \cdots & z_{2P} \\ \vdots & \vdots & \ddots & \vdots \\ z_1^{N-1} & z_2^{N-1} & \cdots & z_{2P}^{N-1} \end{bmatrix} \cdot \begin{bmatrix} B_1 \\ B_2 \\ \vdots \\ B_{2P} \end{bmatrix} \tag{20}$$

where each B_i can be calculated using the total least square method. Furthermore, the initial amplitude A_i and initial phase θ_i can be described by:

$$\begin{cases} A_i = 2\,|B_i| \\ \theta_i = \arctan(\mathrm{Im}(B_i)/\mathrm{Re}(B_i)) \end{cases} \tag{21}$$

After calculating the modal parameters of the signal, the identified LFO signal can be fitted. The index AFI [19] can be used to characterize the approximation degree between the fitting signal and the actual signal. In general, effective mode identification can be accepted while the value of AFI is greater than 10 dB. Otherwise, it is necessary to retry mode identification.

According to the above statement, the whole processing of LFO mode identification using the proposed algorithm is illustrated in Figure 4.

IV. CASE STUDY AND DISCUSSION

In this section, three cases studies with analyses and discussions are presented. The first case study is a simulation of synthetic signal mode identification. The second one analyzes the active power LFO in the IEEE four-generator and two-area system which is tested and validated in the RT-LAB experiment platform. The third one is the oscillation analysis of the actual LFO data in the North American power grid.

A. SIMULATION ON SYNTHETIC SIGNAL MODE IDENTIFICATION

This case study is conducted to test the proposed algorithm using a typical synthetic signal model which is based on the mathematical mode selected and performed in [18]. In this paper, the signal defined in Equation (22) includes two closely spaced modes 0.2284 Hz and 0.2800 Hz. The test signal $s_{syn}(n)$ is discretized with a rate of 100 samples/s and a total observation time of 20 s.

$$\begin{aligned} s_{syn}(n) &= \underbrace{1.0000 \times e^{-0.1697n} \cdot \cos(2\pi \times 0.2284n - 0.8000\pi)}_{\text{mod e\#1}} \\ &+ \underbrace{1.3200 \times e^{-0.8150n} \cdot \cos(2\pi \times 0.6250n + 0.6000\pi)}_{\text{mod e\#2}} \\ &+ \underbrace{1.1300 \times e^{-1.8230n} \cdot \cos(2\pi \times 1.0290n + 0.1000\pi)}_{\text{mod e\#3}} \\ &+ \underbrace{1.0000 \times e^{-0.1697n} \cdot \cos(2\pi \times 0.2800n - 0.8000\pi)}_{\text{mod e\#4}} \end{aligned} \tag{22}$$

where n = 0, 1, 2, . . . , N-1, N = 2000 and $s_{syn}(n)$ is artificially added with noise to be SNR = 15 dB.

Figure 5 shows the synthetic original signal, noisy signal and de-noised signal. The wavelet basis and decomposition level are Coif5 and level 4, respectively in the de-noising method of the wavelet soft-threshold de-noising proposed in this paper. It can be seen that noise reduction processing brings the de-noised signal closer to the original synthetic signal. The SNR and MSE of the de-noised signal are 26.4996 dB and 6.5612×10^{-4}, respectively.

After wavelet soft-threshold de-noising, the adaptive MP algorithm is performed. The model parameters are identified and compared by different algorithms including the proposed method illustrated in Table 5, where T_h represents the threshold value, and the value A_d denotes the adaptive threshold value. T_c is the computing time of 100 realizations for the corresponding algorithm. The computer with an i7-6700 processor of 3.40 GHz, the RAM of 4.0 GB and the 64-bit version of Win10 is chosen for computing.

On the other hand, the fitting LFO signals constructed with the identified parameters in different algorithms are presented

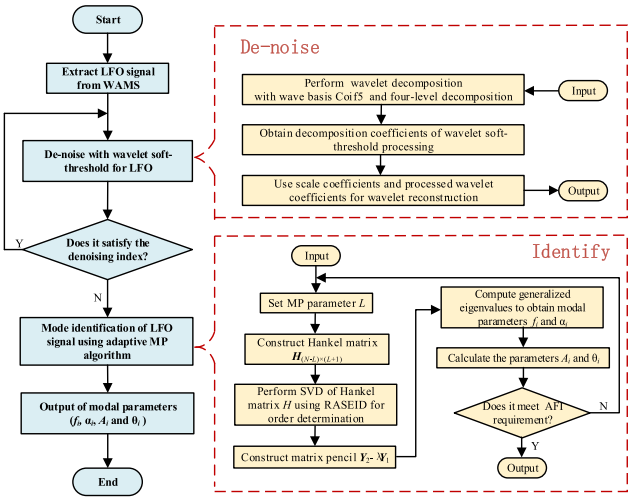

FIGURE 4. Flowchart of the proposed method.

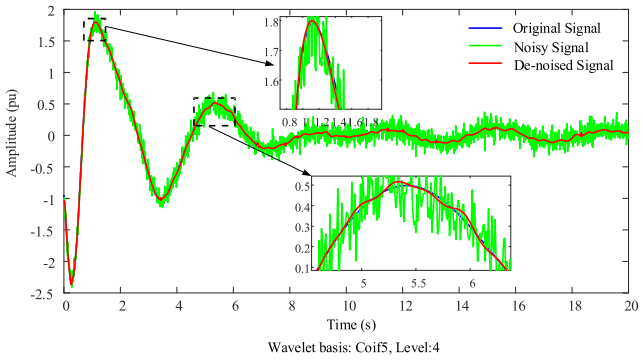

FIGURE 5. Synthetic original signal, noisy signal and de-noised signal.

TABLE 5. Identifying results in different algorithms.

Identifying algorithm	T_h	Modes	f_i (Hz)	α_i	AFI (dB)	Orders	T_c(s)
Prony	0.05	1	0.2923	-0.3048	6.4555	2	1034.7875
TLS-ESPRIT	0.05	3	0.6975 0.2253 0.2861	-1.3527 -0.2221 -0.1262	20.1218	6	49.3562
MP	0.05	3	0.6984 0.2254 0.2852	-1.3485 -0.2181 -0.1280	21.2515	6	122.0281
Proposed algorithm	A_d	4	1.0093 0.6366 0.2820 0.2282	-1.5303 -0.8474 -0.1521 -0.1886	27.9345	8	44.4113

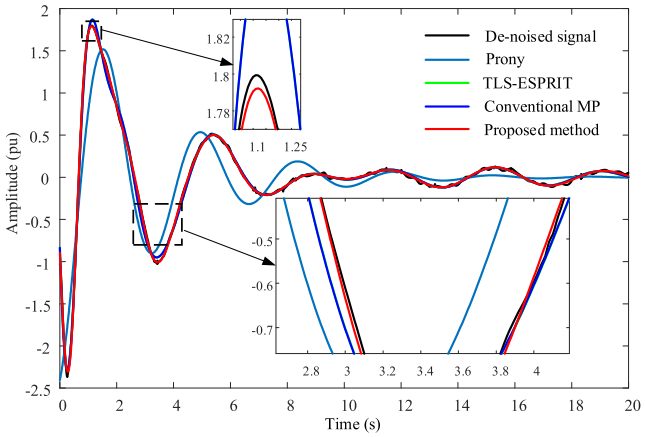

FIGURE 6. The fitting LFO signal curves in different algorithms.

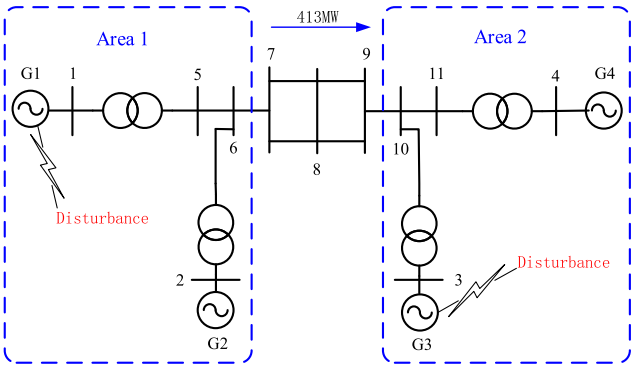

FIGURE 7. The IEEE four-generator and two-area system with disturbance.

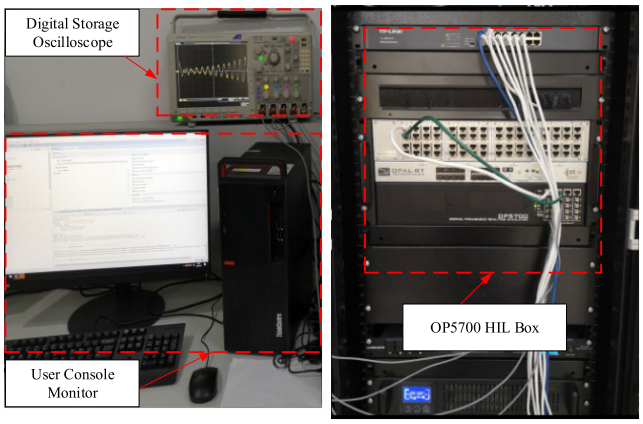

FIGURE 8. RT-LAB experimental setup.

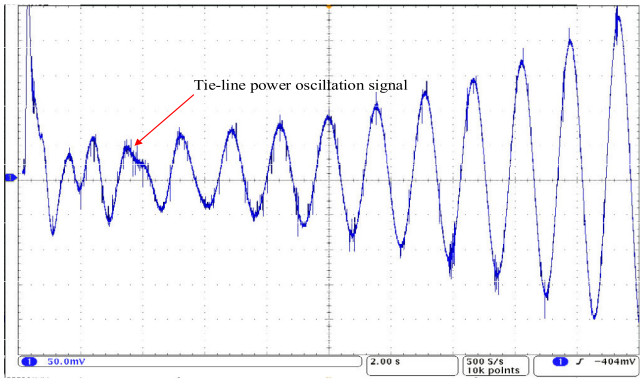

FIGURE 9. Oscilloscope output of the tie-line power oscillation.

in Figure 6. Observing the approximation degree between the de-noised signal and the fitting signals, the adaptive MP algorithm proposed in this paper has an advantage over the others in curve approximation effect and its computing time T_c is rather short and satisfactory.

B. AN EXPERIMENT ON IEEE FOUR-GENERATOR AND TWO-AREA SYSTEM BASED ON RT-LAB EXPERIMENT PLATFORM

In this subsection, the effectiveness of the proposed method is verified by the analysis of the IEEE four-generator and two-area system [3] based on the RT-LAB experiment platform. As described in Figure 7, it is assumed that two areas are connected by double weak tie-lines from point 7 to point 9, and the load of the system is very heavy which is prone to occur LFO. In normal operation, area 1 including G1 and G2 transmits the active power of 413 MW to area 2 including G3 and G4. At the moment t = 1 s, the excitation reference voltage of G1 and G3 is disturbed artificially with 5% of the stable amplitude sustaining a period of 0.1 s.

To validate the performance of the proposed algorithm, the IEEE four-generator and two-area system is accomplished in MATLAB/SIMULINK. Then, the test system containing the disturbances is loaded and performed in the RT-LAB experiment platform [42] including OP5700 hardware-in-loop (HIL) box, digital storage oscilloscope and user console monitor illustrated in Figure 8.

The active power ($\boldsymbol{P}_L$) of the LFO signal which is from point 7 to point 9 of tie-line is obtained between area 1 and area 2 as illustrated in Figure 7. In Figure 9, after removing the DC component, $\boldsymbol{P}_L$ is extracted from the digital storage oscilloscope which is the type MD04104C mixed domain oscilloscope 1 GHz & 5Gs/s. Clearly, the extracted LFO signal in the system carries the white noise which is produced from hardware equipment in the transmission process. It is saved in flash memory and displayed with the data sampling interval of 0.01 s which is intercepted from the time point 1 s as the oscillating start time with the total oscillation period of 16.8 s as shown in Figure 10 (a). According to wavelet soft-threshold de-noising, the de-noised $\boldsymbol{P}_L$ is illustrated in Figure 10 (b) which indicates the noise reduction effect obviously.

The de-noised $\boldsymbol{P}_L$ is shown in Figure 10 (b). The mode identification analysis is carried out by using different identifying algorithms in which the threshold value is uniformly set to be 0.1. The main parameters are calculated and listed in Table 6. In fact, there are two actual LFO modes in the systems which are 1.1137 Hz, -0.4589 and 0.6407 Hz,

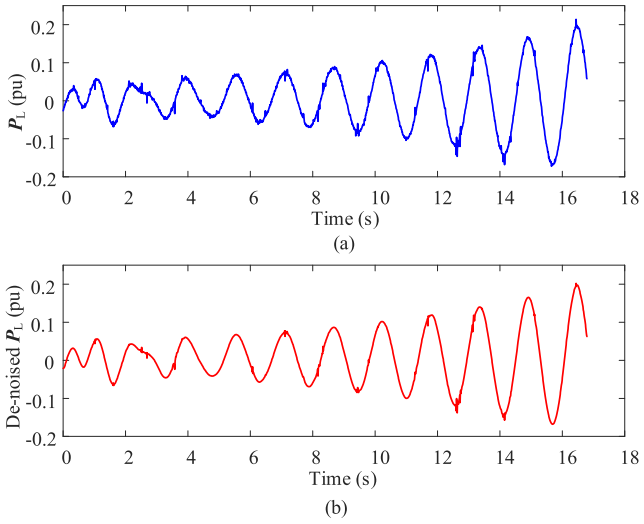

FIGURE 10. (a) P_L, (b) De-noised P_L.

TABLE 6. Identifying parameters and errors of the proposed algorithm.

Method	Mode	Frequency (Hz)	Damping factor	AFI(dB)
Prony	#1	0.6409	0.1106	17.8807
TLS-ESPRIT	#1	0.6410	0.1108	8.3759
MP	#1	0.6410	0.1110	16.7433
Proposed Algorithm	#1	1.1063	-0.4435	30.1375
	#2	0.6409	0.1097	

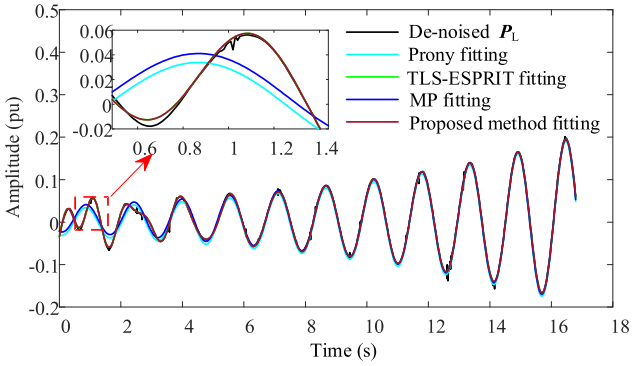

FIGURE 11. Fitting of different algorithms.

0.1087, respectively. Compared to the actual parameters, it can be seen that the proposed algorithm can effectively identify the LFO modes adaptively and calculate the parameters accurately. The fitting curves are described with different algorithms in Figure 11. According to the different fitting curves, the proposed algorithm fitting is the closest one to the de-noised $\boldsymbol{P}_L$.

Furthermore, using different mode identification methods to identify the de-noised $\boldsymbol{P}_L$, Table 7 illustrates that the proposed method is effective to improve the conventional MP

TABLE 7. Comparison of mode identification results of different algorithms.

Method	Threshold	orders	Modes	AFI (dB)	T_c(s)
Prony	0.1	2	1	17.8807	5.7740
	0.05	2	1	17.8807	5.8207
	0.005	5	3	17.8894	5.7976
TLS-ESPRIT	0.1	3	2	8.3759	0.2309
	0.05	5	3	14.7312	0.1778
	0.005	13	7	15.1106	0.1819
MP	0.1	3	2	16.7433	0.3586
	0.05	4	2	29.4724	0.3117
	0.005	14	7	30.3179	0.3280
Proposed method	Adaptive	4	2	30.1375	0.2985

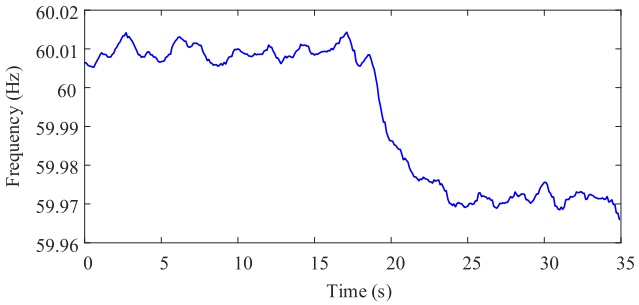

FIGURE 12. The measured frequency signal.

algorithm and has the self-adaptability avoiding the instability of artificial order determination. T_c is the average computing time of 100 realizations for the corresponding method.

C. OSCILLATION ANALYSIS OF NORTH AMERICAN POWER GRID

In this section, the actual power grid data is measured and extracted from the PMU in the North American power grid. This data is utilized to evaluate the effect of the proposed method on identifying the LFO. The LFO is measured at 06:27:35 which is set as the start time point and continues for 35 s in Kansas City, USA. The measured frequency signal is recorded in the PMU and the sampling frequency is 10 Hz, that is, a rate of 10 samples/s and a total observation time of 35 s as shown in Figure 12.

After eliminating the DC and trend components from the measured frequency signal mentioned above, the frequency is de-noised with the proposed de-noising method and described in standard value, as shown in Figure 13.

In Figure 14, a wavelet time-frequency analysis is performed on the de-noised signal as shown in Figure 13. The horizontal axis represents time. The left vertical axis represents the frequency. The color-bar in the right axis indicate the

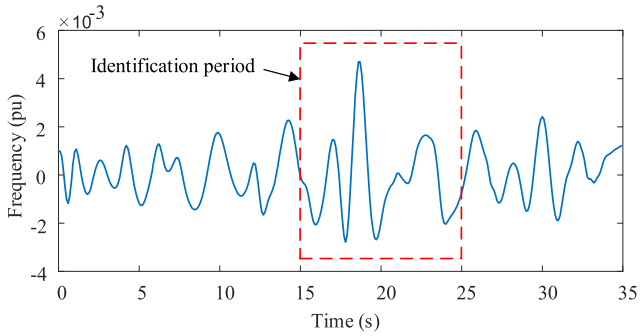

FIGURE 13. De-noised frequency signal without DC and trend components.

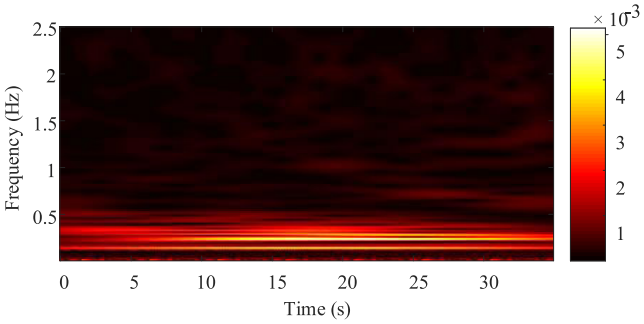

FIGURE 14. Wavelet time-frequency analysis.

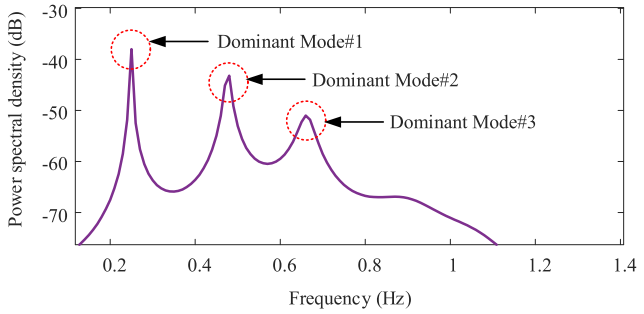

FIGURE 15. The power spectrum density distribution.

energy of time-frequency coordinate point. The high-energy area tends to be golden, and the low-energy area tends to be black. It is found that the highlighted golden area is mainly distributed in the period of 15 s-25 s, which indicates that the frequency fluctuation in this period is relatively violent. Furthermore, the system is disturbed in this period to occur LFO and the measured signal in this period can be taken as the object of LFO analysis. The selected period of the measured signal, which is marked by a dotted box in the period of 15 s and 25 s in the Figure 13, is prepared for the subsequent identification.

Since the number of the LFO modes equals that of the LFO frequency components, it is an effective way to judge the dominant modes according to the composition of the frequency. In order to analyze the composition of the frequency, the oscillation signal is characterized with the power spectral density distribution shown in Figure 15. It can be seen that

TABLE 8. Identification with different choices.

de-noising or not	Identification method	Mode	Frequency (Hz)	Damping factor	Order	AFI(dB)
Without De-noising	Conventional MP	#1	1.5268	-0.1330	30	6.3994
		#2	0.9216	-0.5322		
		#3	0.7163	-0.3543		
	Adaptive MP	#1	0.7326	-0.0119	12	3.0176
		#2	0.5209	-0.0627		
		#3	0.2516	0.1175		
With De-noising	Conventional MP	#1	0.9586	-0.099	10	6.0837
		#2	0.6886	-0.1805		
		#3	0.4980	0.1021		
	Adaptive MP	#1	**0.6559**	**-0.0925**	**6**	**10.4678**
		#2	**0.4851**	**-0.0791**		
		#3	**0.2336**	**0.0732**		

there are sharp peaks in the power spectral density near the frequencies of 0.25 Hz, 0.48 Hz, 0.66 Hz. The three dominant modes are distributed around these three frequency points. Accordingly, the dominant modes of the LFO are determined.

Based on the processing with and without noise respectively, the LFO identifications are performed by conventional MP and adaptive MP based on RASAID. The parameters of the dominant modes are analyzed in different choices and the results are shown in Table 8. It can be seen from Table 8 that there are more accurate model order and parameters of domain frequency and damping factors using the proposed method which contains de-noising and the adaptive MP.

V. CONCLUSION

This paper has proposed a novel adaptive MP algorithm based on wavelet soft-threshold de-noising to deal with the LFO signal extracted from the WAMS in power systems. The proposed algorithm can accurately self-adaptively identify a noisy LFO signal. The main advantage of the proposed de-noising method lies in the appropriate wavelet basis and decomposition level. Moreover, in the proposed adaptive MP algorithm, the RASEID self-adaptively determines the order of SVD, which avoids the influence of the human experience. The cases studies have effectively verified the proposed method. Furthermore, the results have illustrated that the proposed parameters setting wavelet basis Coif5 and decomposition level 4 to noisy LFO signal are more effective comparing to other parameters. Meanwhile, compared to conventional MP and other identifying algorithms listed in literature, the results showed that the proposed adaptive MP algorithm is adaptive and less-sensitive to noise.

REFERENCES

[1] W. Jin and Y. Lu, "Stability analysis and oscillation mechanism of the DFIG–based wind power system," *IEEE Access*, vol. 7, pp. 88937–88948, 2019.

[2] S. C. Chevalier, P. Vorobev, and K. Turitsyn, "Using effective generator impedance for forced oscillation source location," *IEEE Trans. Power Syst.*, vol. 33, no. 6, pp. 6264–6277, Nov. 2018.
[3] Y. Yu, S. Grijalve, and J. Thomas, "Oscillation energy analysis of inter-area low frequency oscillation in power systems," *IEEE Trans. Power Syst.*, vol. 31, no. 2, pp. 1195–1203, Aug. 2016.
[4] T. A. Papadopoulos, A. I. Chrysochos, E. O. Kontis, P. N. Papadopoulos, and G. K. Papagiannis, "Measurement–based hybrid approach for ring-down analysis of power systems," *IEEE Trans. Power Syst.*, vol. 31, no. 6, pp. 4435–4446, Nov. 2016.
[5] F. DeMello and C. Concordia, "Concept of synchronous machine stability as affected by excitation control," *IEEE Trans. Power Appl. Syst.*, vol. 31, no. 6, pp. 316–329, Apr. 1969.
[6] A. Q. Zhang, L. L. Zhang, M. S. Li, and Q. H. Wu, "Identification of dominant low frequency oscillation modes based on blind source separation," *IEEE Trans. Power Syst.*, vol. 32, no. 6, pp. 4774–4782, Nov. 2017.
[7] T. Jin, S. Liu, R. C. Flesch, and W. Su, "A method for the identification of low frequency oscillation modes in power systems subjected to noise," *Appl. Energy*, vol. 206, pp. 1379–1392, Nov. 2017.
[8] L. Simon, K. S. Swarup, and J. Ravishankar, "Wide area oscillation damping controller for DFIG using WAMS with delay compensation," *IET Renew. Power Gener.*, vol. 13, no. 1, pp. 128–137, Jan. 2019.
[9] V. Terzija, G. Valverde, D. Cai, P. Regulski, V. Madani, J. Fitch, S. Skok, M. M. Begovic, and A. Phadke, "Wide–area monitoring, protection, and control of future electric power networks," *Proc. IEEE*, vol. 99, no. 1, pp. 80–93, Jan. 2011.
[10] J. Ma, P. Zhang, H.-J. Fu, B. Bo, and Z.-Y. Dong, "Application of Phasor measurement unit on locating disturbance source for low–frequency oscillation," *IEEE Trans. Smart Grid*, vol. 1, no. 3, pp. 340–346, Dec. 2010.
[11] R. Wies, J. Pierre, and D. Trudnowski, "Use of ARMA block processing for estimating stationary low-frequency electromechanical modes of power systems," *IEEE Trans. Power Syst.*, vol. 18, no. 1, pp. 167–173, Feb. 2003.
[12] T. Hiyama, N. Suzuki, and T. Funakoshi, "On-line identification of power system oscillation modes by using real time FFT," in *Proc. IEEE Power Eng. Soc. Winter Meeting Conf.*, Jan. 2000, pp. 1521–1526.
[13] M. I. Plett, "Transient detection with cross wavelet transforms and wavelet coherence," *IEEE Trans. Signal Process.*, vol. 55, no. 5, pp. 1605–1611, May 2007.
[14] D. Lauria and C. Pisani, "On Hilbert transform methods for low frequency oscillations detection," *IET Gener., Transmiss. Distrib.*, vol. 8, no. 6, pp. 1061–1074, Jun. 2014.
[15] X. Xia, C. Li, and W. Ni, "Dominant low-frequency oscillation modes tracking and parameter optimisation of electrical power system using modified Prony method," *IET Gener., Transmiss. Distrib.*, vol. 11, no. 17, pp. 4358–4364, Nov. 2017.
[16] H. Zeineldin, T. Abdel-Galil, E. El-Saadany, and M. Salama, "Islanding detection of grid connected distributed generators using TLS–ESPRIT," *Electr. Power Syst. Res.*, vol. 77, no. 2, pp. 155–162, Feb. 2007.
[17] K. Sheshyekani, G. Fallahi, M. Hamzeh, and M. Kheradmandi, "A general noise–resilient technique based on the matrix pencil method for the assessment of harmonics and interharmonics in power systems," *IEEE Trans. Power Del.*, vol. 32, no. 5, pp. 2179–2188, Oct. 2017.
[18] R. Schumacher, G. H. Oliveira, and R. Kuiava, "A novel time-domain linear ringdown method based on vector fitting for estimating electromechanical modes," *Electr. Power Syst. Res.*, vol. 160, pp. 300–307, Jul. 2018.
[19] J. Chen, T. Jin, M. A. Mohamed, and M. Wang, "An adaptive TLS–ESPRIT algorithm based on an s–g filter for analysis of low frequency oscillation in wide area measurement systems," *IEEE Access*, vol. 7, pp. 47644–47654, 2019.
[20] J. Khodaparast and M. Khederzadeh, "Least square and Kalman based methods for dynamic phasor estimation: A review," *Protection Control Mod. Power Syst.*, vol. 2, no. 1, pp. 1–18, 2017.
[21] X. He, C. Hu, Y. Hong, L. Shi, and H.-T. Fang, "Distributed Kalman filters with state equality constraints: Time–based and event–triggered communications," *IEEE Trans. Autom. Control*, vol. 65, no. 1, pp. 28–43, Jan. 2020, doi: 10.1109/tac.2019.2906462.
[22] N. E. Huang, Z. Shen, and S. R. Long, "The empirical mode decomposition and the Hilbert spectrum for nonlinear and non-stationary time series analysis," *Proc. Roy. Soc. London. A, Math., Phys. Eng. Sci.*, vol. 454, pp. 903–995, 1998.
[23] Y. Chen, Z. Liu, and H. Liu, "A Method of fiber Bragg grating sensing signal de–noise based on compressive sensing," *IEEE Access*, vol. 6, pp. 28318–28327, 2018.
[24] F. Russo, "Fuzzy systems in instrumentation: Fuzzy signal processing," in *Proc. IEEE Instrum. Meas. Technol. Conf.*, Apr. 1995, pp. 735–740.
[25] H. Su, Z. Fang, and D. Xu, "Trajectory prediction of spinning ball based on fuzzy filtering and local modeling for robotic ping-pong player," *IEEE Trans. Instrum. Meas.*, vol. 62, no. 11, pp. 2890–2900, Nov. 2013.
[26] S. D. Nguyen, S.-B. Choi, and T.-I. Seo, "Recurrent mechanism and impulse noise filter for establishing ANFIS," *IEEE Trans. Fuzzy Syst.*, vol. 26, no. 2, pp. 985–997, Apr. 2018.
[27] J. Serra and L. Vincent, "An overview of morphological filtering," *Circuits Syst. Signal Process*, vol. 11, no. 1, pp. 47–108, Mar. 1992.
[28] J. Yu, T. Hu, and H. Liu, "A new morphological filter for fault feature extraction of vibration signals," *IEEE Access*, vol. 7, pp. 53743–53753, 2019.
[29] D. Donoho, "De-noising by soft-thresholding," *IEEE Trans. Inf. Theory*, vol. 41, no. 3, pp. 613–627, May 1995.
[30] X. Xu, M. Luo, Z. Tan, and R. Pei, "Echo signal extraction method of laser radar based on improved singular value decomposition and wavelet threshold denoising," *Infr. Phys. Technol.*, vol. 92, pp. 327–335, Aug. 2018.
[31] N. A. Golilarz, H. Gao, and W. Ali, "Hyper-spectral remote sensing image de-noising with three dimensional wavelet transform utilizing smooth nonlinear soft thresholding function," in *Proc. 15th Int. Comput. Conf. Wavelet Active Media Technol. Inf. Process. (ICCWAMTIP)*, Dec. 2018, pp. 142–146.
[32] Z. Alyasseri, A. Khader, M. Al-Betar, and M. A. Awadallah, "Hybridizing β-hill climbing with wavelet transform for denoising ECG signals," *Inf. Sci.*, vol. 429, pp. 229–246, Mar. 2018.
[33] F. M. Bayer, A. J. Kozakevicius, and R. J. Cintra, "An iterative wavelet threshold for signal denoising," *Signal Process.*, vol. 162, pp. 10–20, Sep. 2019.
[34] A. Messina, V. Vittal, G. Heydt, and T. Browne, "Nonstationary approaches to trend identification and denoising of measured power system oscillations," *IEEE Trans. Power Syst.*, vol. 24, no. 4, pp. 1798–1807, Nov. 2009.
[35] C.-C. Liao, H.-T. Yang, and H.-H. Chang, "Denoising techniques with a spatial noise–suppression method for wavelet–based power quality monitoring," *IEEE Trans. Instrum. Meas.*, vol. 60, no. 6, pp. 1986–1996, Jun. 2011.
[36] H. Zhang, H. Liu, and J. Fang, "Online current signal de-noising of magnetic bearing switching power amplifier based on lifting wavelet transform," *IET Electr. Power Appl.*, vol. 10, no. 8, pp. 799–806, Sep. 2016.
[37] M. M. A. Nezhadi, H. Hassanpour, and F. Zare, "Grid impedance estimation using low power signal injection in noisy measurement condition based on wavelet denoising," in *Proc. 2017 3rd Iranian Conf. Intell. Syst. Signal Process. (ICSPIS)*, Dec. 2017, pp. 81–86.
[38] S. K. Jain and S. N. Singh, "Exact model order ESPRIT technique for harmonics and interharmonics estimation," *IEEE Trans. Instrum. Meas.*, vol. 61, no. 7, pp. 1915–1923, Jul. 2012.
[39] S. K. Jain, P. Jain, and S. N. Singh, "A fast harmonic Phasor measurement method for smart grid applications," *IEEE Trans. Smart Grid*, vol. 8, no. 1, pp. 493–502, Jan. 2017.
[40] Y. Hua, K. Tapan, and Sarkar, "Matrix pencil method for estimating parameters of exponentially admped/undamped sinusoids in noise," *IEEE Trans. Acoust., Speech, Signal Process.*, vol. 38, no. 5, pp. 814–824, May 1990.
[41] Y. Hua and T. Sarkar, "On SVD for estimating generalized eigenvalues of singular matrix pencil in noise," *IEEE Trans. Signal Process.*, vol. 39, no. 4, pp. 892–900, Apr. 1991.
[42] R. K. Patjoshi and K. Mahapatra, "High-performance unified power quality conditioner using command generator tracker-based direct adaptive control strategy," *IET Power Electron.*, vol. 9, no. 6, pp. 1267–1278, May 2016.

JIAN CHEN received the B.S. degree from the School of Physics and Electronics, Center South University, China, in 2004, and the M.S. degree from the College of Electrical and Information Engineering, Hunan University, China, in 2011. He is currently pursuing the Ph.D. degree with the Department of Electrical Engineering, Fuzhou University.

From 2005 to 2009, he was a Research Assistant with the Hunan Institute of Technology, Hengyang, China, where he was a Lecturer and a Senior Experimenter, from 2012 to 2016. His research interests include power system automation technology and artificial intelligence.

XIN LI received the B.S. degree from the School of Electrical and Information Engineering, Xiangtan University, China, in 2002, and the M.S. degree from the College of Computer and Communications, Hunan University, China, in 2012. From 2005 to 2009, she was a Research Assistant with the Hunan Institute of Technology, Hengyang, China, where she has been a Lecturer, since 2010. Her research interests include computer algorithm and artificial intelligence.

MOHAMED A. MOHAMED (Member, IEEE) received the B.Sc. and M.Sc. degrees from Minia University, Minia, Egypt, in 2006 and 2010, respectively, and the Ph.D. degree from King Saud University, Riyadh, Saudi Arabia, in 2016. He joined the College of Electrical Engineering and Automation, Fuzhou University, China, as a Postdoctoral Research Fellow, in 2018. He has been a faculty member with the Department of Electrical Engineering, College of Engineering, Minia University, since 2008. He has supervised multiple M.Sc. and Ph.D. theses, worked on a number of technical projects, and published various articles and books. His current research interests include renewable energy, energy management, power electronics, power quality, optimization, smart islands, and smart grids. He has also joined the editorial board of some scientific journals and steering committees of many international conferences.

TAO JIN (Senior Member, IEEE) was born in Hubei, China, in 1976. He received the B.S. and M.S. degrees from Yanshan University, in 1998 and 2001, respectively, and the Ph.D. degree in electrical engineering from Shanghai Jiao Tong University, in 2005. From 2005 to 2007, he held postdoctoral position with Shanghai Jiao Tong University. During this time, he was in charge of a research group in the biggest dry-type transformer company in Asia, Sunten Electrical Company Ltd., to develop new transformer technology with distribution grid. From 2008 to 2009, he held research scientist position with Virginia Tech, Blacksburg, USA, where he was involved in the design and test of PMU technology and GPS/internet-based power system frequency monitoring network. In 2010, he joined Imperial College London, U.K., as European Union Marie Curie Research Fellow, where he was focused on electrical technologies related to smart grid. He is currently a Professor with the College of Electrical Engineering and Automation, Fuzhou University, China. He has published about 110 articles.

Dr. JIN is a member of the IEEE Power and Energy Society and the IEEE Industrial Electronics Society, and a special committee member of Chinese Society of Electrical Engineering and China Electrotechnical Society. He currently serves as an Associate Editor for China *Measurement & Testing Technology* and other journals.